# NOTES AND CORRESPONDENCE

## A Method to Determine the Capping Inversion of the Convective Boundary Layer

G. RAMPANELLI AND D. ZARDI

*Dipartimento di Ingegneria Civile ed Ambientale, Università degli studi di Trento, Trento, Italy*

11 July 2003 and 20 December 2003

ABSTRACT

A simple mathematical algorithm is proposed to decipher the thermal structure of the convective boundary layer by means of best-fit analysis of soundings or airborne measurements with a smooth ideal profile. The latter includes a constant-potential-temperature mixed layer, a strongly stratified entrainment layer, and a constant-lapse-rate free atmosphere. The resulting profile depends on five parameters amenable, through simple mathematical relationships, to physical variables defining the vertical structure of the layers. The method allows objective evaluation of parameters involved in the test profile and easy comparison of measurements with theoretically expected structure.

### 1. Introduction

Various simplified schemes have been proposed in the literature to model the vertical profile of potential temperature in the situation illustrated in Fig. 1. The latter reproduces the thermal structure of a convective boundary layer (CBL): the mixed layer (ML) below is connected to the stably stratified free atmosphere (FA) above through the entrainment layer (EL) or ''interfacial layer'' (Deardorff 1979). Key parameters to describe this structure are the potential temperature in the ML $\theta_m$, inversion height $h_0$, entrainment-layer depth $\Delta h$, inversion strength $\Delta\theta$, and lapse rate in the free atmosphere $\gamma$.

Previous models (e.g., Deardorff 1979) capture the essential overall dynamics and diurnal evolution of the CBL without explicit reference to turbulence at smaller scales. In particular, the EL is modeled either as a layer displaying constant stability with rapid temperature variation between the ML and the FA (''first-order jump;'' cf. Betts 1974; Deardorff 1979), or as a sharp temperature discontinuity (''zero-order jump;'' cf. Ball 1960; Tennekes 1973; Betts 1973; Carson 1973; Carson and Smith 1974; Driedonks 1982). This approach allowed for a more comprehensive investigation of the various processes governing the diurnal evolution of an inversion-capped CBL (Zilitinkevich 1975; Tennekes 1973; Deardorff 1979; Fedorovich and Mironov 1985).

*Corresponding author address:* Dino Zardi, Università degli studi di Trento, Dipartimento di Ingegneria Civile ed Ambientale, via Mesiano 77, I-38050 Trento, Italy.
E-mail: dino.zardi@ing.unitn.it

However, these theoretical results are not easily compared with either high-resolution model output (Khanna and Brasseur 1997) or field observations (Boers and Eloranta 1986; Cohn and Angevine 2000). A method for making such a comparison has been recently proposed using airborne lidar data (Davis et al. 2000). Likewise four different criteria to identify the CBL structure from large-eddy simulation models have been suggested by Sullivan et al. (1998).

On the other hand, making a precise estimate of many quantities, such as boundary layer depth (Vogelezang and Holtslag 1996; Gryning et al. 1997), is a crucial step not only for applications (e.g., estimate of mixing height for pollutant transport) but also for evaluating theoretical similarity solutions as these quantities enter as scaling variables (Stull 1988; Johansson et al. 2000).

In order to describe the vertical structure of a CBL from a sounding or model output in terms of the conceptual model sketched in Fig. 1, a best-fit analysis with a simple test vertical profile (such as the curve in Fig. 1) may seem like a reasonable procedure. However, the usual least squares approach, using a piecewise constant test curve where both heights ($h_s$, $h_0$, $h_2$) and thermal structure parameters ($\Delta\theta$, $\gamma$) are unknown quantities, does not lead to an analytical solution, but rather it requires an iterative search. It can be shown that in many cases multiple combinations of the parameters may get close to a minimum scatter of data around the test profile, but the solution producing the absolute minimum may not provide the most reasonable result from a physical viewpoint. On the contrary, a smooth test curve displaying regular merging of each layer into the ad-

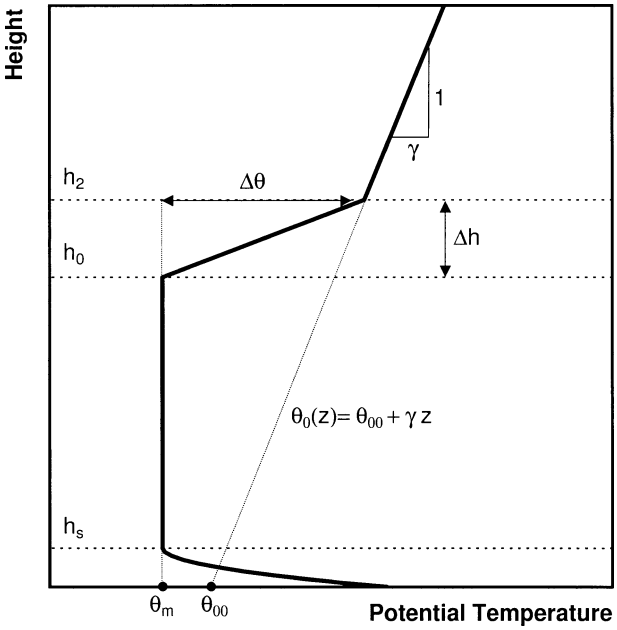


FIG. 1. Sketch of a vertical profile of potential temperature in the convective boundary layer developing over flat uniform terrain [adapted from Garratt (1992); notation for $h_0$ and $h_2$ follows Deardorff (1979)].

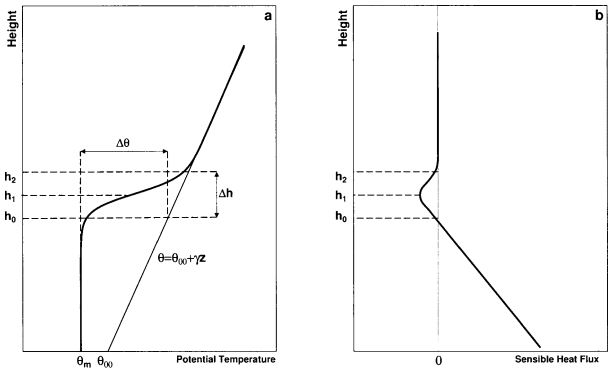


FIG. 2. (a) The smoothed vertical profile of potential temperature and the symbols used in the present paper, associated with (b) the vertical structure of the sensible heat flux.

jacent ones, not only allows for a partly analytical solution of the minimization problem, but is also more likely to avoid ambiguity. Furthermore, as remarked by Deardorff (1979), a piecewise linear profile is a very rough approximation of the smooth transition from each layer to those adjacent to it, because it leaves out various finescale features. A similar strategy has been followed by Fitzjarrald and Garstang (1981) and more recently by Steyn et al. (1999) for the analysis of lidar backscatter profiles.

In the present paper the smooth-test-curve approach is adopted (section 2) and relationships between mathematical parameters defining the curve and the physical variables defining the CBL are determined. Tests with real data are provided (section 3), along with a discussion of the results and possible refinements of the method (section 4).

## 2. Outline of the method

Following Deardorff (1979), the lowest part of a horizontally homogeneous CBL (apart from the surface layer region) can be represented as a layer displaying a constant potential temperature $\theta_m$ up to a height $h_0$, then a rapidly increasing profile in the EL and asymptotically approaching, above a height $h_2$, the free atmosphere,

$$\theta_0(z) = \theta_{00} + \gamma z, \tag{1}$$

where $\theta_{00}$ is a constant value of potential temperature at reference height ($z = 0$) and $\gamma$ is the constant vertical gradient. The height $h_1$ is where the vertical heat flux profile displays a minimum (Fig. 2). Such a structure may be easily reproduced by means of a linear combination of functions in the form

$$\theta(z) = \theta_m + af(\eta) + bg(\eta), \tag{2}$$

where

$$\eta = \frac{z - l}{c\Delta h} \tag{3}$$

is the vertical displacement from a reference height $l$ (to be related later to the CBL height) scaled with the EL depth $\Delta h$ and $c$ is a constant (to be specified later). The structure of $f$ and $g$ is sketched in Fig. 3: the function $f$ provides the rapid transition from the constant value $\theta_m$, as $\eta \ll 0$, to a value of $\theta$ at the top of the EL, matching the FA above, while the function $g$ provides the correct asymptotic behavior in accordance with (1) as $\eta \gg 0$.

Accordingly, the following constraints have to be satisfied:

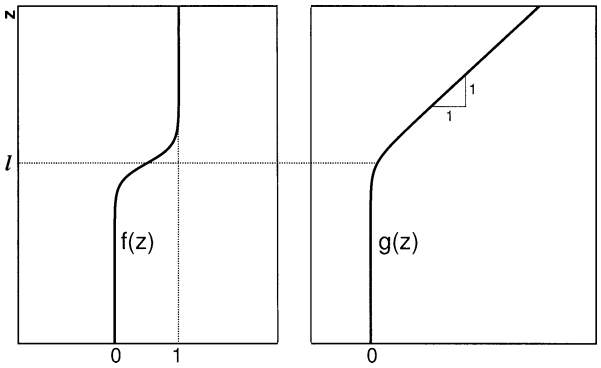


FIG. 3. Sketch of the basic functions $f$ and $g$ used in (2) to obtain the vertical profile.

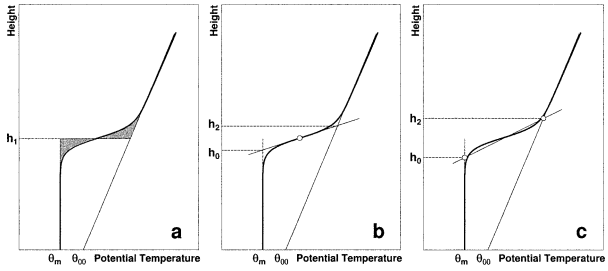


FIG. 4. Summary of criteria for the identification of standard meteorological parameters: (a) shaded areas are equal as a consequence of energy budget (Driedonks 1982), (b) linear potential temperature profile displaying the same lapse rate as the gradient of the real profile at the inflection point, and (c) evaluation of heights at which the best-fit profile is close enough either to the ML constant value $\theta_m$ ($h_0$) or to the FA ($h_2$).

$$\lim_{\eta\to-\infty} \theta(\eta) = \theta_m \Rightarrow \lim_{\eta\to-\infty} f(\eta), g(\eta) = 0, \quad (4)$$

$$\lim_{\eta\to+\infty} f(\eta) = 1, \quad \text{and} \quad (5)$$

$$\lim_{\eta\to+\infty} \frac{dg}{dz} = 1. \quad (6)$$

As will be clear later, the limit value of 1 in (5) and (6) is chosen for convenience, but any constant value would be acceptable. Asymptotic matching with the free atmosphere requires, using (1), (5), and (6),

$$\lim_{\eta\to+\infty} \frac{d\theta}{dz} = \lim_{\eta\to+\infty} \frac{1}{c\Delta h}\left(a\frac{df}{d\eta} + b\frac{dg}{d\eta}\right) = \gamma, \quad (7)$$

which implies

$$b = c\gamma\Delta h. \quad (8)$$

Among the many possible analytic functions satisfying the above requirements, consider the following expressions:

$$f(\eta) = \frac{\tanh(\eta) + 1}{2} \quad \text{and} \quad (9a)$$

$$g(\eta) = \frac{\ln[2\cosh(\eta)] + \eta}{2}. \quad (9b)$$

Equations (1), (2), (9a), and (9b), along with the required asymptotic behavior of $\theta(z)$ in the FA, imply

$$\theta_{00} = \theta_m + a - \gamma l. \quad (10)$$

To link the parameters $a$, $b$, $\theta_m$, $l$, and $\Delta h$ to all of the physical variables identifying the atmospheric-layer structure as shown in Fig. 1, some criteria have to be chosen to compare the smooth profile of (2) with the usual conceptual schemes (Fig. 2). A first criterion based on the energy budget (Driedonks 1982) requires that the shaded areas in Fig. 4a be equal. A second criterion is based on the averaged stability in the EL: accordingly, the best approximation is a linear potential temperature profile displaying a lapse rate equal to the gradient in the real profile at the inflection point (Fig. 4b). A third criterion is based on evaluation of the heights at which the best-fit profile is close enough either to the ML constant value $\theta_m$ ($h_0$), or to the FA ($h_2$) (Fig. 4c). In the following, the latter criterion will be adopted.

The upper ($h_2$) and lower ($h_0$) limit of the EL can be calculated by imposing that the value of $\theta$ at that height must be very close to the asymptotic value, namely,

$$\theta(h_2) \approx \theta_{00} + \gamma h_2 \quad \text{and} \quad (11a)$$

$$\theta(h_0) \approx \theta_m. \quad (11b)$$

This can be obtained by setting

$$h_2 = l + \xi c\Delta h \quad \text{and} \quad (12a)$$

$$h_0 = l - \xi c\Delta h, \quad (12b)$$

where $\xi$ is a parameter related to the depth of the entrainment layer, setting the accuracy within which (11a) and (11b) are satisfied. For large values of $\xi$, the differences between $\theta(h_2)$ and the asymptotic expression in the mixed layer and in the free atmosphere are very small, but this is verified only at heights very high in the FA or very close to the ground level. On the other hand, low values of $\xi$ lead one to estimate a very thin EL, with $\Delta h$ vanishing as $\xi$ approaches 0. On the basis of many applications of expression (2) to real data, a value of $\xi = 1.5$ is recommended as a good compromise. This leads to a very strict fulfillment of (11a) and (11b). The actual depth of the EL can be calculated from (12a) and (12b) as

$$\Delta h \equiv h_2 - h_0 = 2\xi c\Delta h, \quad (13)$$

which implies $c = 1/(2\xi) = 1/3$.

The relationships between the parameters $a$, $b$, and $l$ in (2) and (3), and physical quantities resulting from the above reasoning, are summarized in the following equations:

$$\gamma = \frac{2b}{\Delta h}, \quad (14)$$

$$h_0 = l - \Delta h/2, \quad \text{and} \quad (15)$$

$$\theta_{00} = a + \theta_m - \gamma l = a + \theta_m - \frac{2b}{\Delta h}l. \quad (16)$$

The evaluation of the inversion strength requires some explanation, because it has been variously defined in the literature. The potential temperature jump ($\Delta\theta$) across the EL is

$$\Delta\theta = \theta_{00} + \gamma h_2 - \theta_m = a + b. \quad (17)$$

Betts (1974) suggests for the inversion strength the expression

$$\Delta\theta' = \theta_{00} + \gamma h_1 - \theta_m, \quad (18)$$

assuming $h_1$ to be both the height where the mixed layer is upper bounded by the EL ($h_0$ in the present paper), and the height where turbulent heat flux displays a min-

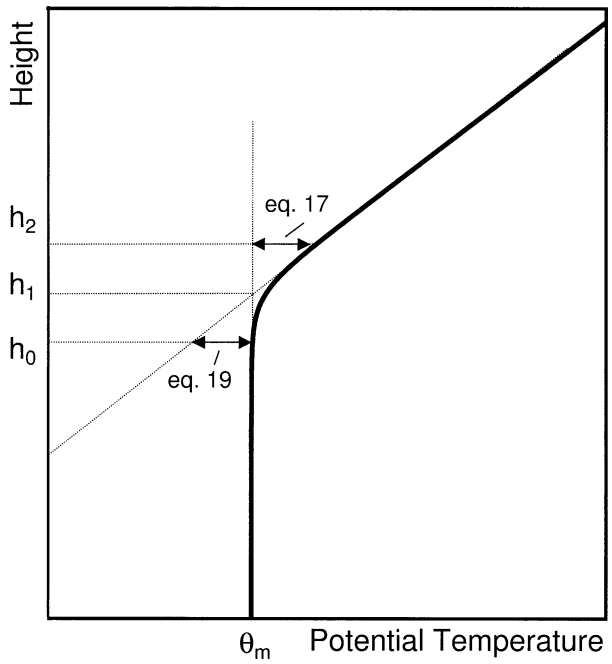


FIG. 5. Sketch of the case of pure encroachment and its interpretation with (17) and (19).

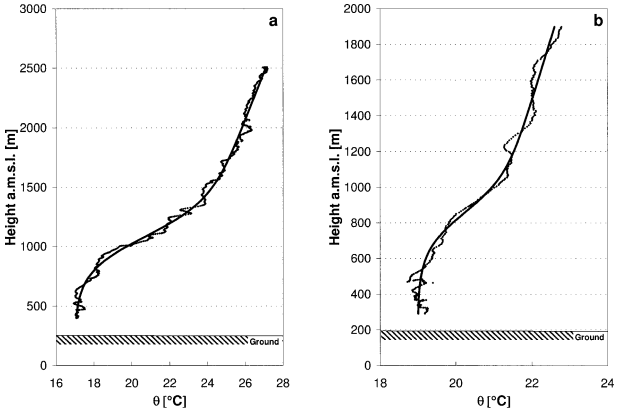


FIG. 6. An example of the analysis of airborne data using the method outlined in the paper. Data were collected in the Adige valley, near the village of Besenello, south of the city of Trento (Italy) during the measurement flights. (a) between 0930 and 0946 LST 1 Oct 1999 and (b) between 0935 and 0948 LST 26 May 1999.

imum. In fact, Deardorff (1979) shows that in general the two heights are different. Accordingly in the following, $h_0$ will denote the height of the inversion base, whereas $h_1$ will denote the heat flux minimum height (Fig. 2).

Straightforward application of (18) in the present case—in which a smooth temperature profile is adopted, using $h_0$ instead of $h_1$ (as stated above)—leads to

$$\Delta\theta' = \theta_{00} + \gamma h_0 - \theta_m = a - b. \tag{19}$$

However, (19) would produce unphysical negative values for $\Delta\theta'$ (see Fig. 5) in the limiting case of *encroachment* (cf. Garratt 1992, p. 151; Stull 1988, p. 454). According to Deardorff (1979), $h_1$ is roughly halfway between $h_0$ and $h_2$. Thus, an optimal compromise should be reached by estimating $h_1 = (h_0 + h_2)/2 = l$, and consequently

$$\Delta\theta' = \theta_{00} + \gamma h_1 - \theta_m = a. \tag{20}$$

Thus, the limiting case of encroachment (i.e., $\Delta\theta/\gamma h_1 \approx 0$; cf. Deardorff 1979) is recovered for vanishing $a$, when the only contribution of the curve $g(\eta)$ in (2) survives (see Figs. 3 and 5). The case of pure encroachment will occur as $a = 0$, as a limiting case that is rarely met in real data. For this reason a value of $a = 0.2$ may be suggested as an upper limit for an encroachment condition.

The estimate of the parameters in (2) can be obtained by the usual least squares fit to the sounding data, requiring the functional

$$S = \sum_1^N [\theta_i - \theta(\eta_i)]^2 \tag{21}$$

to be a minimum; here, $\theta_i$ is the value measured at height $\eta_i = (z_i - l)/c\Delta h$, $\theta(\eta_i)$ is the value of potential temperature calculated from (2) at the same height, and $N$ is the total number of data points. In particular, by minimizing $S$ the optimal values of $a$, $b$, and $\theta_m$ can be related analytically to the values of $l$ and $\Delta h$ (see the appendix).

## 3. Application

The method presented above has been applied to data collected through airborne measurements in the atmospheric boudary layer, allowing for a very easy determination of the parameters identifying the atmospheric thermal structure at the sites of interest. Data have been collected in alpine valleys using an equipped motor glider during various measurement flights in the area surrounding the city of Trento in the Alps (northern Italy). Further details on the instruments and the measurements can be found in de Franceschi et al. (2003).

The vertically spiraling path performed by the motor glider produced an essentially vertical sounding. A few major deviations from a standard vertical sounding are related to horizontal displacements from a strictly vertical ascent and to the occurrence of significant cross-valley temperature gradients, in connection with different sidewall exposure to incoming solar radiation and related thermally driven flows (cf. Whiteman 1990). In spite of these drawbacks the method allows for efficient retrieval of a horizontally averaged basic vertical structure and provides the first step for subsequent analysis of local cross-valley perturbations, as shown in Rampanelli and Zardi (2000, 2002).

In Figs. 6–9 vertical profiles of potential temperature data from diurnal survey flights are shown. Figures 6,

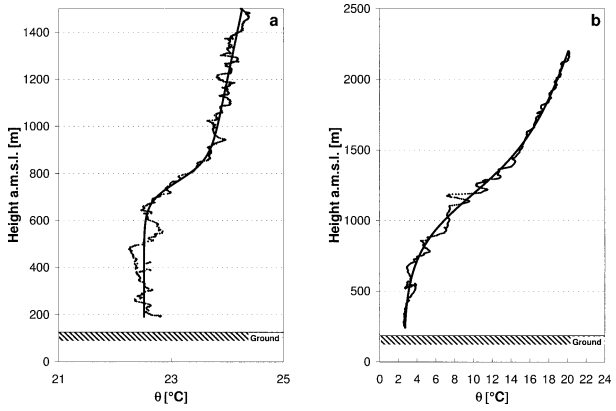


FIG. 7. An example of the analysis of airborne data using the method outlined in the paper. Data were collected in the Adige valley, near the city of Trento (Italy), during the measurement flights (a) between 1023 and 1039 LST 2 Jul 1997 and (b) between 1039 and 1104 LST 22 Dec 2000.

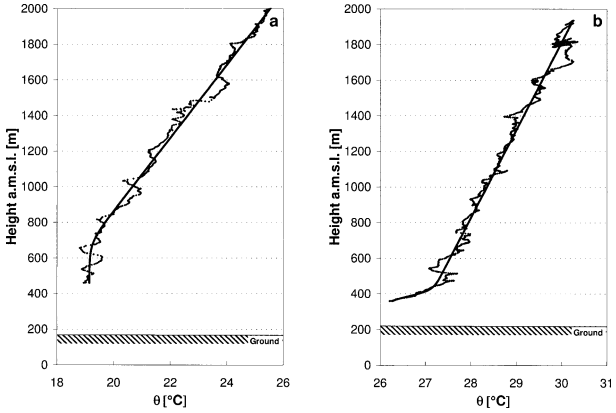


FIG. 9. An example of the analysis of airborne data using the method outlined in the paper. Data were collected during the measurement flight (a) between 1217 and 1229 LST 24 Oct 1998 near the town of Riva del Garda, in the lower Lakes Valley, about 30 km southwest of the city of Trento (Italy), and during the measurement flight (b) between 0932 and 0958 LST 8 Jul 1999 in the Adige valley, near the city of Bolzano (Italy).

7, and 8 display examples of strong and deep entrainment layers capping a shallow mixed layer. These are consistent with what is usually found in deep mountain valleys. A detailed analysis of physical mechanisms governing the diurnal evolution of thermal structure within valleys can be found in Whiteman (1990) and Whiteman et al. (1996). Figures 9a,b show how the method performs under ''worst'' cases, such as (a) ''anomalous'' CBL development (the so-called encroachment) and (b) a ground-based inversion. Both cases are relatively well captured using the proposed method. In fact, for Fig. 9a the algorithm produces a very small inversion strength ($\Delta\theta' = -0.09$ K), identifying this case as an encroachment, and the transition zone between $h_0$ and $h_2$ is well localized and meaningful. In Fig. 9b the flight was performed in the early morning: the height $h_0$ turns out to be less than the height of the lowest measurement point of the profile, and $h_2$ is only about 100 m higher. This suggests that the overall profile is characterized by a single layer, associated with a typical stable condition of a ground-based inversion. The values of the parameters $h_0$, $h_2$, $\Delta h$, $\theta_m$, $\theta_{00}$, $\gamma$, $\Delta\theta$, and $\Delta\theta'$ obtained from the analysis of these data are reported in Tables 1 and 2. In the same tables the correlation coefficient of the best fit is also shown. The general mean vertical structure provided by the dataset is well captured by the resulting continuous profile and the values of parameters defining the vertical structure appear to be in a reasonable range.

Whenever vertical profiles of other variables, such as water vapor content $q$, are measured simultaneously with the thermal profile, a similar approach can be followed to design a shape function, such as (2), for $q$. This function, specifically shaped for the water vapor content structure, can be used to fit the $q$ data and recover the stratification parameters that can be inferred from its profile. A separate fit for each profile ($\theta$ and $q$) is likely to produce different estimates of the same parameters, such as $h_0$ and $h_2$. To overcome this problem and to strengthen the estimate of the parameters, a simultaneous fit is recommended, possibly by minimizing

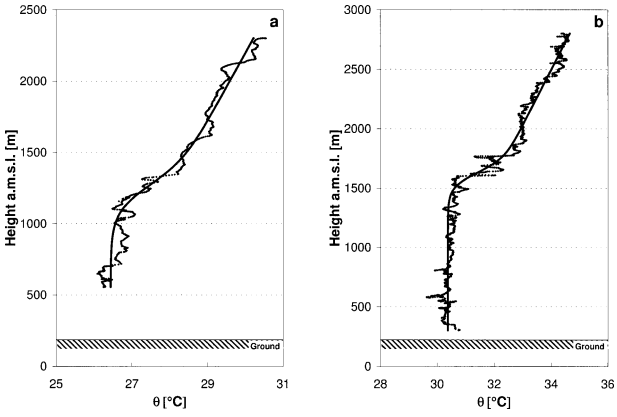


FIG. 8. An example of the analysis of airborne data using the method outlined in the paper. Data were collected in the upper Lakes Valley, near the village of Terlago, west of the city of Trento (Italy), during the measurement flight (a) between 1248 and 1304 LST 9 Sep 1998 and (b) between 1420 and 1452 LST 23 Sep 2001.

TABLE 1. Parameters of the vertical profiles obtained from data shown in Figs. 6–7.

| Variable | Fig. 6a | Fig. 6b | Fig. 7a | Fig. 7b |
|---|---|---|---|---|
| $\Delta h$ (m) | 1070 | 644 | 272 | 1254 |
| $h_0$ (m) | 585 | 517 | 628 | 525 |
| $h_2$ (m) | 1555 | 1161 | 900 | 1780 |
| $\theta_m$ (K) | 290.1 | 292.1 | 295.6 | 275.7 |
| $\theta_{00}$ (K) | 295.6 | 292.9 | 296.1 | 281.4 |
| $\gamma$ (K km$^{-1}$) | 1.41 | 1.45 | 0.88 | 5.38 |
| $\Delta\theta$ (K) | 7.63 | 2.53 | 1.21 | 15.36 |
| $\Delta\theta'$ (K) | 6.79 | 2.07 | 1.09 | 11.98 |
| $R^2$ | 0.996 | 0.990 | 0.976 | 0.980 |

TABLE 2. Parameters of the vertical profiles obtained from data shown in Figs. 8–9.

| Variable | Fig. 8a | Fig. 8b | Fig. 9a | Fig. 9b |
|---|---|---|---|---|
| $\Delta h$ (m) | 581 | 375 | 259 | 105 |
| $h_0$ (m) | 961 | 1435 | 574 | 330 |
| $h_2$ (m) | 1542 | 1811 | 833 | 436 |
| $\theta_m$ (K) | 299.6 | 303.5 | 292.3 | 299.2 |
| $\theta_{00}$ (K) | 298.6 | 305.2 | 288.9 | 299.5 |
| $\gamma$ (K km$^{-1}$) | 2.09 | 3.29 | 4.86 | 2.02 |
| $\Delta\theta$ (K) | 2.19 | 2.23 | 0.71 | 1.16 |
| $\Delta\theta'$ (K) | 1.58 | 1.75 | 0.09 | 1.05 |
| $R^2$ | 0.978 | 0.980 | 0.989 | 0.976 |

the sum of the two functionals that calculate the distance of the theoretical profiles to the data. Obviously, each of these functions has to be normalized in order that there be an equal effect of the information associated with each profile (see the appendix). A comparison between the method of the coupled fit and the method of the single fit is shown in Figs. 10 and 11, and the results are given in detail in Tables 3 and 4. Notice that the differences between the results produced by the two procedures are very small. However, the coupled method uses a larger number of data points to estimate the inversion parameters $l$ and $\Delta h$, and this obviously produces a more stable and reliable result. For this reason, when a coupled series of measurements ($\theta$ and $q$) are available, the application of the coupled procedure is recommended.

## 4. Summary

A new technique to obtain the vertical structure of potential temperature from data collected within and above a CBL using light airplanes or vertical soundings has been introduced. The technique consists of a least squares fitting of data to a user-defined analytical expression. The adjustable parameters of this expression are amenable to the atmospheric variables generally used for the description of the stratification (i.e., inversion height, entrainment depth, mixed layer potential temperature, and free-atmosphere lapse rate).

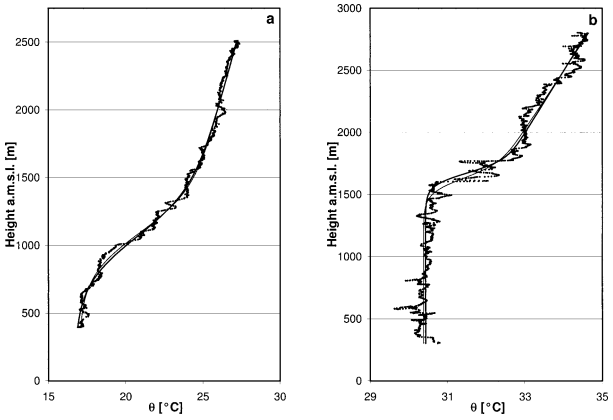


FIG. 10. An example of the analysis of airborne data using the method of the coupled fit using the vertical profiles of both $\theta$ and $q$. Vertical profiles of $\theta$ are shown: data (black dots), interpretation using single fit to the $\theta$ data (thin line), and interpretation using $\theta$–$q$ coupled fit (thick line). Data were collected during the measurement flight of (a) Fig. 6a, and during the measurement flight of (b) Fig. 8b.

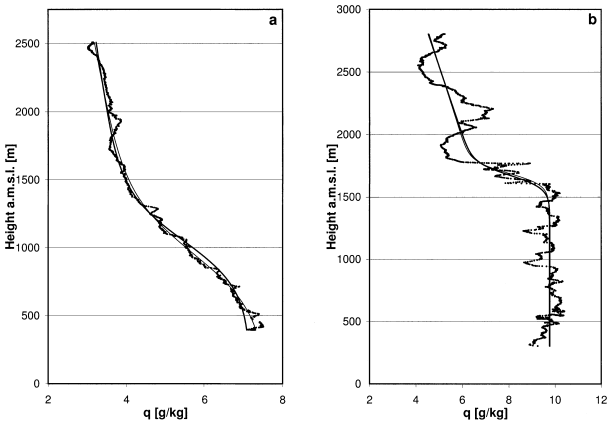


FIG. 11. An example of the analysis of airborne data using the method of the coupled fit using the vertical profiles of both $\theta$ and $q$. Vertical profiles of $q$ are shown: data (black dots), interpretation using single fit to the $q$ data (thin line), and interpretation using $\theta$–$q$ coupled fit (thick line). Data were collected during the measurement flight of (a) Fig. 6a, and during the measurement flight of (b) Fig. 8b.

Application of the technique to real data produces encouraging results. Furthermore, the conditions used for obtaining the suggested expression of the vertical profile are very general, and can be adopted to calculate other expressions for $f(\eta)$ and $g(\eta)$ as well.

As a final comment, we note that the suggested method assumes the database to be reasonably amenable to the basic structure of a capping inversion because it is most commonly found. More complicated structures, such as multiple inversions, could be only poorly reproduced by the method. Possible application of the proposed profile in simplified models for the diurnal evolution of the mixing height (Seibert et al. 2000) could improve the method introducing a more realistic capping inversion structure. An integration with similar methods for the identification of the CBL upper structure from other kinds of measurements (lidar, wind profilers, so-

TABLE 3. Parameters of the vertical profiles obtained from data shown in Fig. 10, and comparison between the single- and coupled-fit procedure.

| Variable | Fig. 10a single fit | Fig. 10a coupled fit | Fig. 10b single fit | Fig. 10b coupled fit |
|---|---|---|---|---|
| $\Delta h$ (m) | 1070 | 1083 | 375 | 310 |
| $h_0$ (m) | 585 | 496 | 1435 | 1513 |
| $h_2$ (m) | 1555 | 1579 | 1811 | 1823 |
| $\theta_m$ (K) | 290.1 | 289.8 | 303.5 | 303.5 |
| $\theta_{00}$ (K) | 295.6 | 294.9 | 305.2 | 305.4 |
| $\gamma$ (K km$^{-1}$) | 1.41 | 1.70 | 3.29 | 2.49 |
| $\Delta\theta$ (K) | 7.63 | 7.77 | 2.23 | 2.28 |
| $\Delta\theta'$ (K) | 6.79 | 6.93 | 1.75 | 1.90 |
| $R^2$ | 0.996 | 0.995 | 0.980 | 0.976 |

TABLE 4. Parameters of the vertical profiles obtained from data shown in Fig. 11, and comparison between the single- and coupled-fit procedure.

| Variable | Fig. 10a single fit | Fig. 10a coupled fit | Fig. 10b single fit | Fig. 10b coupled fit |
|---|---|---|---|---|
| $\Delta h$ (m) | 1321 | 1083 | 284 | 310 |
| $h_0$ (m) | 274 | 496 | 1544 | 1513 |
| $h_2$ (m) | 1595 | 1579 | 1828 | 1823 |
| $q_m$ (g kg$^{-1}$) | 7.5 | 7.2 | 9.7 | 9.7 |
| $q_{00}$ (g kg$^{-1}$) | 5.0 | 4.4 | 6.5 | 6.8 |
| $q$ (g kg$^{-1}$ km$^{-1}$) | −0.60 | −0.36 | −0.19 | −0.22 |
| $\Delta q$ (g kg$^{-1}$) | −3.3 | −3.3 | −3.54 | −3.51 |
| $\Delta q'$ (g kg$^{-1}$) | −3.1 | −3.1 | −3.27 | −3.17 |
| $R^2$ | 0.994 | 0.990 | 0.929 | 0.928 |

dar, etc.) is possible, in order to obtain a more accurate knowledge of the physical variables.

*Acknowledgments.* Special thanks go to Massimiliano de Franceschi, for providing the experimental setup of the motor glider and technical support for the measurements, and to the motor glider pilots, Andrea Ferrari and Fabrizio Interlandi. This work has been partly supported by the Provincia Autonoma di Trento under Project PAT-UNITN 2001, and by granting a leave of absence to G. Rampanelli for completing his Ph.D. program. This work has been also partly supported by the Italian National Institute for Scientific and Technological Research on the Mountain under the program INRM2000.

## APPENDIX

### Minimizing the Functional *S*

For the estimation of the parameters $a$, $b$, $\theta_m$, $l$, and $\Delta h$ in (2), the usual least squares method requires that the function

$$S = \sum_1^N [\theta_i - \theta(\eta_i)]^2 \tag{A1}$$

be a minimum, where $\theta_i$ is the value measured at height $\eta_i$, $\theta(\eta_i)$ is the value of the vertical profile at the same height, and $N$ is the total number of data. The minimum requirement can be imposed by setting

$$\frac{\partial}{\partial \theta_m}\sum_1^N [\theta_i - \theta(\eta_i)]^2 = 0,$$

$$\frac{\partial}{\partial a}\sum_1^N [\theta_i - \theta(\eta_i)]^2 = 0,$$

$$\frac{\partial}{\partial b}\sum_1^N [\theta_i - \theta(\eta_i)]^2 = 0,$$

$$\frac{\partial}{\partial \Delta h}\sum_1^N [\theta_i - \theta(\eta_i)]^2 = 0, \quad \text{and}$$

$$\frac{\partial}{\partial l}\sum_1^N [\theta_i - \theta(\eta_i)]^2 = 0; \tag{A2}$$

then

$$\sum_1^N [\theta_i - \theta(\eta_i)]\frac{\partial \theta}{\partial \theta_m}(\eta_i) = 0, \tag{A3a}$$

$$\sum_1^N [\theta_i - \theta(\eta_i)]\frac{\partial \theta}{\partial a}(\eta_i) = 0, \tag{A3b}$$

$$\sum_1^N [\theta_i - \theta(\eta_i)]\frac{\partial \theta}{\partial b}(\eta_i) = 0, \tag{A3c}$$

$$\sum_1^N [\theta_i - \theta(\eta_i)\frac{\partial \theta}{\partial \Delta h}(\eta_i) = 0, \quad \text{and} \tag{A3d}$$

$$\sum_1^N [\theta_i - \theta(\eta_i)]\frac{\partial \theta}{\partial l}(\eta_i) = 0. \tag{A3e}$$

Note that the terms (A3d) and (A3e) depend on the specific structure of the functions $g$ and $f$, while by the definition provided in (2) we have

$$\frac{\partial \theta}{\partial \theta_m}(\eta_i) = 1, \tag{A4a}$$

$$\frac{\partial \theta}{\partial a}(\eta_i) = f(\eta_i), \quad \text{and} \tag{A4b}$$

$$\frac{\partial \theta}{\partial b}(\eta_i) = g(\eta_i), \tag{A4c}$$

therefore, (A4a)–(A4c) become simply

$$\sum_1^N [\theta_i - \theta(\eta_i)] = 0,$$

$$\sum_1^N [\theta_i - \theta(\eta_i)]f(\eta_i) = 0, \quad \text{and}$$

$$\sum_1^N [\theta_i - \theta(\eta_i)]g(\eta_i) = 0, \tag{A5}$$

which upon substitution from (2) and rearrangements gives

$$\theta_m N + a\sum_1^N f(\eta_i) + b\sum_1^N g(\eta_i) = \sum_1^N \theta_i,$$

$$\theta_m \sum_1^N f(\eta_i) + a\sum_1^N f^2(\eta_i) + b\sum_1^N g(\eta_i)f(\eta_i) = \sum_1^N \theta_i f(\eta_i), \quad \text{and}$$

$$\theta_m \sum_1^N g(\eta_i) + a\sum_1^N f(\eta_i)g(\eta_i) + b\sum_1^N g^2(\eta_i) = \sum_1^N \theta_i g(\eta_i), \tag{A6}$$

which is a linear symmetric algebraic system in the variables $a$, $b$, and $\theta_m$. Once the system is solved, $a$, $b$, and $\theta_m$ are directly related to $l$ and $\Delta\eta$, which are the only free parameters left to be varied to minimize $S$.

In the case of a coupled fit using vertical profiles of potential temperature and water vapor content, the function to be minimized is

$$S = \sum_1^N \left[\frac{\theta_i - \theta(\eta_i)}{\Theta}\right]^2 + \sum_1^N \left[\frac{q_i - q(\eta_i)}{Q}\right]^2, \quad \text{(A7)}$$

where $q_i$ is the $q$ value measured at height $\eta_i$, $q(\eta_i)$ is the value of the vertical profile of water vapor content at the same height, $\Theta$ and $Q$ are two suitable scaling factors (suggested values are the span of $\theta$ and of $q$ in the vertical profile under analysis). According to Stull (1988) and Garratt (1992), the shape function of the vertical profile of water vapor content can be assumed in the form

$$q(z) = q_m + a_q f(\eta) + b_q g(\eta), \quad \text{(A8)}$$

with the functions $f$ and $g$ identical to those used for the $\theta$ profile. Obviously, the linear behavior of (A8) in the FA can produce negative values of water vapor when $z$ is very large, but (A8) can be used as a linear approximation of the vertical profile for the lower region of the FA. The minimum requirement of $S$ can be imposed by setting

$$\frac{\partial}{\partial \theta_m}\sum_1^N [\theta_i - \theta(\eta_i)]^2 = 0,$$

$$\frac{\partial}{\partial a}\sum_1^N [\theta_i - \theta(\eta_i)]^2 = 0,$$

$$\frac{\partial}{\partial b}\sum_1^N [\theta_i - \theta(\eta_i)]^2 = 0,$$

$$\frac{\partial}{\partial q_m}\sum_1^N [q_i - q(\eta_i)]^2 = 0,$$

$$\frac{\partial}{\partial a_q}\sum_1^N [q_i - q(\eta_i)]^2 = 0,$$

$$\frac{\partial}{\partial b_q}\sum_1^N [q_i - q(\eta_i)]^2 = 0,$$

$$\frac{\partial}{\partial \Delta h}\left\{\sum_1^N \frac{[\theta_i - \theta(\eta_i)]^2}{\Theta^2} + \sum_1^N \frac{[q_i - q(\eta_i)]^2}{Q^2}\right\} = 0, \quad \text{and}$$

$$\frac{\partial}{\partial l}\left\{\sum_1^N \frac{[\theta_i - \theta(\eta_i)]^2}{\Theta^2} + \sum_1^N \frac{[q_i - q(\eta_i)]^2}{Q^2}\right\} = 0; \quad \text{(A9)}$$

then

$$\sum_1^N [\theta_i - \theta(\eta_i)]\frac{\partial \theta}{\partial \theta_m}(\eta_i) = 0, \quad \text{(A10a)}$$

$$\sum_1^N [\theta_i - \theta(\eta_i)]\frac{\partial \theta}{\partial a}(\eta_i) = 0, \quad \text{(A10b)}$$

$$\sum_1^N [\theta_i - \theta(\eta_i)]\frac{\partial \theta}{\partial b}(\eta_i) = 0, \quad \text{(A10c)}$$

$$\sum_1^N [q_i - q(\eta_i)]\frac{\partial q}{\partial q_m}(\eta_i) = 0, \quad \text{(A10d)}$$

$$\sum_1^N [q_i - q(\eta_i)]\frac{\partial q}{\partial a_q}(\eta_i) = 0, \quad \text{(A10e)}$$

$$\sum_1^N [q_i - q(\eta_i)]\frac{\partial q}{\partial b_q}(\eta_i) = 0, \quad \text{(A10f)}$$

$$\sum_1^N \frac{[\theta_i - \theta(\eta_i)]}{\Theta^2}\frac{\partial \theta}{\partial \Delta h}(\eta_i) + \sum_1^N \frac{[q_i - q(\eta_i)]}{Q^2}\frac{\partial q}{\partial \Delta h}(\eta_i) = 0, \quad \text{and (A10g)}$$

$$\sum_1^N \frac{[(\theta_i - \theta(\eta_i)]}{\Theta^2}\frac{\partial \theta}{\partial l}(\eta_i) + \sum_1^N \frac{[q_i - q(\eta_i)]}{Q^2}\frac{\partial q}{\partial l}(\eta_i) = 0. \quad \text{(A10h)}$$

The terms (A10g) and (A10h), as in the single fit procedure, depend on the specific structure of the functions $g$ and $f$, but even in this case we have

$$\frac{\partial q}{\partial q_m}(\eta_i) = 1, \qquad \frac{\partial q}{\partial a_q}(\eta_i) = f(\eta_i), \quad \text{and}$$

$$\frac{\partial q}{\partial b_q}(\eta_i) = g(\eta_i); \quad \text{(A11)}$$

therefore, (A10a)–(A10f) after splitting and rearrangements become simply

$$\theta_m N + a\sum_1^N f(\eta_i) + b\sum_1^N g(\eta_i) = \sum_1^N \theta_i,$$

$$\theta_m \sum_1^N f(\eta_i) + a\sum_1^N f^2(\eta_i) + b\sum_1^N g(\eta_i) f(\eta_i) = \sum_1^N \theta_i f(\eta_i),$$

$$\theta_m \sum_1^N g(\eta_i) + a\sum_1^N f(\eta_i) g(\eta_i) + b\sum_1^N g^2(\eta_i) = \sum_1^N \theta_i g(\eta_i), \quad \text{(A12)}$$

$$q_m N + a_q\sum_1^N f(\eta_i) + b_q\sum_1^N g(\eta_i) = \sum_1^N q_i,$$

$$q_m \sum_1^N f(\eta_i) + a_q\sum_1^N f^2(\eta_i) + b_q\sum_1^N g(\eta_i) f(\eta_i) = \sum_1^N q_i f(\eta_i), \quad \text{and}$$

$$q_m \sum_1^N g(\eta_i) + a_q \sum_1^N f(\eta_i)g(\eta_i) + b_q \sum_1^N g^2(\eta_i) = \sum_1^N q_i g(\eta_i). \quad \text{(A13)}$$

These are two uncoupled linear symmetric algebraic systems with the variables $a$, $b$, $\theta_m$ and $a_q$, $b_q$, $q_m$, respectively.

Once these two systems are solved, $a$, $b$, $\theta_m$ and $a_q$, $b_q$, $q_m$ are directly related to $l$ and $\Delta h$, as in the case of the single fit to only one variable. This second procedure produces a single estimate for $l$ and $\Delta h$ for the vertical profiles of both potential temperature and water vapor content. An example is shown in Figs. 10 and 11 using the data displayed in Figs. 6a and 8b. The results are reported in Tables 3 and 4, for a comparison with the single-fit procedure.

## REFERENCES


Ball, F. K., 1960: Control of inversion height by surface heating. *Quart. J. Roy. Meteor. Soc.*, **86,** 483–494.

Betts, A. K., 1973: Non-precipitating cumulus convection and its parameterization. *Quart. J. Roy. Meteor. Soc.*, **99,** 178–196.

——, 1974: Reply to comment on the paper ''Non-precipitating cumulus convection and its parameterization.'' *Quart. J. Roy. Meteor. Soc.*, **100,** 469–471.

Boers, R., and E. W. Eloranta, 1986: Lidar measurements of the atmospheric entrainment zone and the potential temperature jump across the top of the mixed layer. *Bound.-Layer Meteor.*, **34,** 357–375.

Carson, D. J., 1973: The development of a dry inversion-capped convectively unstable boundary layer. *Quart. J. Roy. Meteor. Soc.*, **99,** 450–467.

——, and F. B. Smith, 1974: Thermodynamic model for the development of a convectively unstable boundary layer. *Advances in Geophysics*, Vol. 18A, Academic Press, 111–124.

Cohn, S. A., and W. M. Angevine, 2000: Boundary layer height and entrainment zone thickness measured by lidars and wind-profiling radars. *J. Appl. Meteor.*, **39,** 1233–1247.

Davis, K. J., N. Gamage, C. R. Hagelberg, C. Kiemle, D. H. Lenshow, and P. P. Sullivan, 2000: An objective method for deriving atmospheric structure from airborne lidar observations. *J. Atmos. Oceanic Technol.*, **17,** 1455–1468.

Deardorff, J. W., 1979: Prediction of convective mixed-layer entrainment for realistic capping inversion structure. *J. Atmos. Sci.*, **36,** 424–436.

de Franceschi, M., G. Rampanelli, D. Sguerso, D. Zardi, and P. Zatelli, 2003: Developement of a measurement platform on a light airplane and analysis of airborne measurements in the atmospheric boundary layer. *Ann. Geophys.*, **46,** 1–15.

Driedonks, A. G. M., 1982: Models and observations of the growth of the atmospheric boundary layer. *Bound.-Layer Meteor.*, **23,** 283–306.

Fedorovich, E. E., and D. V. Mironov, 1995: A model for shear-free convective boundary layer with parameterized capping inversion structure. *J. Atmos. Sci.*, **52,** 83–95.

Fitzjarrald, D. R., and M. Garstang, 1981: Vertical structure of the tropical boundary layer. *Mon. Wea. Rev.*, **109,** 1512–1526.

Garratt, J. R., 1992: *The Atmospheric Boundary Layer*. Cambridge University Press, 316 pp.

Gryning, S. E., F. Beyrich, and E. Batchvarova, Eds., 1997: The determination of the mixing height—Current progress and problems. *EURASAP Workshop Proc.*, Roskilde, Denmark, Risø National Laboratories, 157 pp.

Johansson, C., A. S. Smedman, and U. Högström, 2000: Critical test of the validity of Monin–Obukhov similarity during convective conditions. *J. Atmos. Sci.*, **58,** 1549–1566.

Khanna, S., and J. G. Brasseur, 1997: Analysis of Monin–Obukhov similarity from large-eddy simulation. *J. Fluid Mech.*, **345,** 251–286.

Rampanelli, G., and D. Zardi, 2000: Analysis of airborne data and identification of thermal structures with geostatistical techniques. Preprints, *14th Symp. on Boundary Layers and Turbulence*, Aspen, CO, Amer. Meteor. Soc., 239–241.

——, and ——, 2002: Identification of thermal structure from airborne measurements in an Alpine valley with kriging technique. Preprints, *10th Conf. on Mountain Meteorology*, Park City, UT, Amer. Meteor. Soc., 1.20–1.24.

Seibert, P., F. Beyrich, S.-E. Gryning, S. Joffre, A. Rasmussen, and P. Tercier, 2000: Review and intercomparison of operational methods for the determination of the mixing height. *Atmos. Environ.*, **34,** 1001–1027.

Steyn, D. G., M. Baldi, and R. M. Hoff, 1999: The detection of mixed layer depth and entrainment zone thickness from lidar backscatter profiles. *J. Atmos. Oceanic Technol.*, **16,** 953–959.

Stull, R. B., 1988: *An Introduction to Boundary Layer Meteorology*. Kluwer Academic, 670 pp.

Sullivan, P. P., C.-H. Moeng, B. Stevens, D. H. Lenschow, and S. D. Mayor, 1998: Structure of the entrainment zone capping the convective atmospheric boundary layer. *J. Atmos. Sci.*, **55,** 3042–3064.

Tennekes, H., 1973: A model for the dynamics of the inversion above a convective boundary layer. *J. Atmos. Sci.*, **30,** 558–567.

Vogelezang, D. H. P., and A. A. M. Holtslag, 1996: Evaluation and model impacts of alternative boundary-layer height formulations. *Bound.-Layer Meteor.*, **81,** 245–269.

Whiteman, C. D., 1990: Observations of thermally developed wind sytems in mountainous terrain. *Atmospheric Processes over Complex Terrain, Meteor. Monogr.*, No. 23, Amer. Meteor. Soc., 5–42.

——, T. B. McKee, and J. C. Doran, 1996: Boundary layer evolution within a canyonland basin. Part I: Mass, heat, and moisture budgets from observations. *J. Appl. Meteor.*, **35,** 2145–2161.

Zilitinkevich, S. S., 1975: Comments on ''A model for the dynamics of the inversion above a convective boundary layer.'' *J. Atmos. Sci.*, **32,** 991–992.